European Polymer Journal 193 (2023) 112105

Contents lists available at ScienceDirect

European Polymer Journal

journal homepage: www.elsevier.com/locate/europolj

In vitro electrically controlled amoxicillin release from 3D-printed chitosan/bismuth ferrite scaffolds

Dilruba Baykara [a,b], Esra Pilavci [a,c], Songul Ulag [a,d,*], Oseweuba Valentine Okoro [e], Lei Nie [f], Amin Shavandi [e], Ayse Ceren Koyuncu [a,d], Ozlem Bingol Ozakpinar [g], Mehmet Eroglu [a], Oguzhan Gunduz [a,d]

[a] Center for Nanotechnology and Biomaterials Application & Research (NBUAM), Marmara University, Istanbul, Turkey
[b] Department of Bioengineering, Faculty of Chemistry and Metallurgy, Yildiz Technical University, Turkey
[c] Institute of Pure and Applied Sciences, Department of Metallurgical and Materials Engineering Marmara University, Istanbul, Turkey
[d] Department of Metallurgical and Materials Engineering, Faculty of Technology, Marmara University, Istanbul, Turkey
[e] BioMatter unit - École polytechnique de Bruxelles, Université Libre de Bruxelles (ULB), Avenue F.D. Roosevelt, 50 - CP 165/61, 1050 Brussels, Belgium
[f] College of Life Sciences, Xinyang Normal University (XYNU), Xinyang 464000, China
[g] Department of Basic Pharmaceutical Sciences, Faculty of Pharmacy, Marmara University, Istanbul, Turkey

ARTICLE INFO

Keywords:
Amoxicillin
Bismuth ferrite
Chitosan
Controlled drug delivery
Scaffold
3D printing

ABSTRACT

The goal of this study was to design and fabricate a 3D-printed wound dressing using chitosan as a bioink, with the ability to release the antibiotic drug amoxicillin (AMX) in response to mild electrical stimulation. This was achieved through the incorporation of bismuth ferrite (BFO) nanoparticles, which have both magnetic and ferroelectric properties. The chitosan-based scaffolds containing various concentrations of BFO were analyzed using Fourier transform infrared spectroscopy, and the release of AMX from the scaffolds was evaluated *in vitro* under electrical stimulation. The results demonstrated that the scaffolds had a suitable structure for drug loading and release, and the release of AMX was successfully controlled by the applied electrical stimulus. The maximum tensile strength (4.97 ± 0.34 MPa) was observed at the ratio of 6% CHT/0.025% BFO scaffolds and the scaffold with 6% CHT/0.075% BFO had the maximum cell viability of (~130%) at 168 h incubation time. This study highlights the potential of BFO to deliver therapeutic drugs from a 3D-printed chitosan scaffold in a controlled manner.

1. Introduction

Designing a wound dressing for use in skin tissue engineering requires detailed optimization of its properties considering the extent, shape, and pathophysiology of the injury. A wound dress must provide a moist environment, as well as allow gas exchange and be mechanically compatible with the native skin tissue. Besides, additional therapeutics could be required at the site of injury caused by burns, trauma, or surgical operations. Wound dressings with porous architecture can be designed to carry such therapeutic drugs to the desired area, promoting healing while favoring cell attachment, proliferation, and tissue formation. One such method involves using three-dimensional (3D) printing technology to fabricate structures with custom internal microarchitecture [1]. This technology incorporates novel materials (i.e. natural or synthetic) in the design of cell-laden bioinks which can contain drug substances to promote wound treatment and management. The versatility and repeatability provided by 3D printing technology allow us to overcome the shortcomings of traditional biofabrication methods. Three-dimensional scaffolds comprised of artificial and organic polymers have been created using a variety of techniques, including gas foaming, melt molding, electrospinning, and phase separation. Nevertheless, these scaffold production techniques cannot precisely alter the scaffold's shape, inner channel arrangement, or pore size. The severe processing conditions of these approaches also prevent the production of scaffolds containing cells [2].

The technology also facilitates the 3D-printed of skin and the engineering of skin substitutes or scaffolds that allow drug loading [3]. The development of magnetically responsive scaffolds is based on the blending of polymer gels with magnetic nanoparticles, enabling the modulation of drug and cell delivery at the target wound area [3].

* Corresponding author at: Center for Nanotechnology and Biomaterials Application & Research (NBUAM), Marmara University, Istanbul, Turkey.
E-mail address: songul.ulag@marmara.edu.tr (S. Ulag).

https://doi.org/10.1016/j.eurpolymj.2023.112105
Received 9 February 2023; Received in revised form 2 April 2023; Accepted 24 April 2023
Available online 30 April 2023

Bismuth ferrite (BFO), a multiferroic material with both magnetic and ferroelectric properties at room temperature, can be formed as a drug carrier whose release profile could be controlled with electrical induction [4]. Controlled release and targeted delivery of drugs reduce the side effects that can arise from excessive use while providing a sustained release of drugs. Due to the ongoing emergence of bacterial resistance, numerous studies on the subject of antimicrobial studies in metal-based NPs are crucial to nanomedicine. The compounds with bismuth ferrite nanoparticles can increase activity by adding additional materials. Many studies have reported the associated antibacterial activity of BFO nanoparticles that is size/shape dependent [5]. A recent study shows that the antibacterial activity of amoxicillin (AMX), one of the most commonly used antibacterial drugs, could be maintained for at least 6 weeks using a novel controlled drug delivery system for skin tissue [6]. Our paper demonstrates the feasibility of controlling the release of AMX from BFO nanoparticles *in vitro* by electricity.

For the engineering of skin tissue, natural hydrogels are generally preferred due to their ability to maintain a moist environment while supporting the cells that would regenerate the tissue. Chitosan (CHT) is a natural polymer that can be obtained by partial deacetylation of chitin from sea crustaceans. It is biocompatible and non-allergic, and it can absorb water up to 3 times its weight [7], making it one of the most commonly preferred hydrogel bioink for 3D printing in soft tissue engineering studies. Moreover, chitosan is highly effective in wound healing as it speeds up tissue formation, [8] and research shows that low molecular weight chitosan prevents microbial growth by inhibiting bacterial gene expression [9].

Herein, the aim of this article is to develop chitosan-based wound dressing materials that carry drugs that can be triggered electrically. Wound dressing materials containing BFO-AMX nanoparticles in different proportions were produced using a 3d printer. Electrically triggered drug release has the potential to create a new perspective for regeneration. In addition, these scaffolds can be used according to the needs of the patient and contribute to the personalized treatment method. With the ability to adjust the delivery rate in accordance with the patient's needs, the electrically triggered delivery of AMX from CHT/BFO scaffolds may open up new possibilities for regeneration as well as the individualized therapy of many diseases. To our knowledge, this study is the first to investigate the effect of BFO nanoparticles on AMX release from 3D-printed chitosan-based scaffolds via mild electrical stimulation. The main novelty of this study is due to the presence of BFO and the encapsulation of the drug into the BFO at the synthesis stage. In addition, these drug encapsulated particle was added into the CHT scaffold to observe the release control with both the degradation of CHT and electric stimulation. There are some studies about the investigation of electric stimulation to drug release [10,11] but fabrication of AMX encapsulated BFO and BFO-added 3D-printed CHT scaffolds are the new study for the literature. After the fabrication process, the chemical, morphological, mechanical and thermal characteristics of the scaffolds were investigated. Then, electrical drug release and cell biocompatibility were investigated by *in vitro* studies.

2. Materials and methods

2.1. Materials

Bismuth (III) nitrate ($Bi_5O(OH)_9(NO_3)_4$, MW = 1.461,99 g/mol), iron (III) nitrate nonahydrate ($Fe(NO_3)_3$, MW = 403.95 g/mol), dichloromethane (DCM), and nitric acid (65%) were purchased from Merck KGaA, Germany. Ammonia solution (25%, MW = 35.05 g/mol) was supplied from ISOLAB (Wertheim, Germany). Chitosan (low molecular weight, deacetylated chitin) was purchased from Sigma Aldrich (USA). Acetic acid glacial (CH_3COOH, M = 60.05 g/mol) was obtained by Merck, Germany, and amoxicillin (96%) was supplied from Acros Organics.

2.2. BFO synthesis

BFO nanoparticles were obtained using a co-precipitation route method. Firstly, 2.58 g iron nitride [Fe $(NO_3)_3{\cdot}9H_2O$] was dissolved in the distilled water (10 ml) at the magnetic stirrer at 300 rpm for 15 min. Then, 1.86 g bismuth nitride (Bi $(NO_3)_3.5H_20$) was dissolved in the 10 ml nitric acid for half an hour at the stirrer with the same rpm. The two solutions were dissolved entirely and stirred in the same beaker for 15 min to obtain a homogeneous mixture. In this step, 20 mg of AMX was added to this mixture to get drug-loaded BFO nanoparticles. When the mixture reached transparency, an ammonia solution was added to the mixture to control the pH to obtain a precipitate. The preparation of the precursor and co-precipitation solutions was performed at room temperature. The resulting precipitate was passed through the filter paper and washed with distilled water to remove the toxic effect of the agents. Then, the powders were put in the oven for 24 h at 100 °C to evaporate the water in them [12].

2.3. Preparation of the solutions

6% chitosan (w/v) was dissolved in 2% acetic acid aqueous solution at 80°in a magnetic stirrer for 30 mins [13]. After completely dissolving chitosan, drug-loaded BFO particles were added to the solution at ratios 0.025%, 0.05%, and 0.075%, respectively. The solutions were ready for the 3D printing process.

2.4. Fabrication of the 3D printed scaffolds

The scaffold was designed using CAD software. The 3D scaffolds were fabricated using a 3D printer device (Hyrel 3D, SDS-5 Extruder, GA, USA). Hydrogels were loaded into a 10 ml syringe. The syringe was connected to the 30 Ga needle and placed on the head of the printer. 3D printing was performed at a printing speed of 10 mm/s, the flow rate of 1 ml/h. The scaffold had a square shape of 20 mm × 20 mm × 1 mm dimensions. The other parameters were set as follows: the infill density = 60%, the total layer = 8, and the infill pattern was rectangular. At the end of the printing process, all scaffolds were put in sodium 8% NaOH solution for 5 min for crosslinking.

2.5. Characterization of the scaffolds

2.5.1. Fourier transform infrared spectroscopy (FT-IR)

The molecular structures of the scaffolds were analyzed by using Fourier transform infrared spectroscopy (FTIR, 4700 Jasco, Japan). The results of the spectrum were analyzed at a scanning range of 450–4000 cm^{-1} and a resolution of 4 cm^{-1}.

2.5.2 Scanning Electron Microscopy (SEM) and Transmission Electron Microscope (TEM)

BFO powder was dissolved in methanol using a sonicator to prepare samples for TEM (HITACHI HT7800), which were then placed onto copper grids covered in carbon. The morphological analysis of the scaffolds was examined using SEM (EVA MA 10, ZEISS, USA). The surface of the scaffolds was coated with Au with a coating machine (Quorum SC7620, ABD). The average pore sizes of scaffolds were measured using software (Analysis5, Olympus, USA).

2.5.3. Differential scanning calorimeter (DSC)

The thermal properties of the 3D-printed scaffolds were determined by using a DSC (Shimadzu DSC 60 Plus, Japan). The temperature ranges were adjusted from 25 °C to 600 °C at the scanning rate of 10 °C/min.

2.5.4. Mechanical properties of the scaffolds

The tensile properties of the scaffolds were analyzed using a tensile test machine (SHIMADZU, EZ-LX, CHINA). Before the tensile test, the thickness of the scaffolds was measured using a digital micrometer

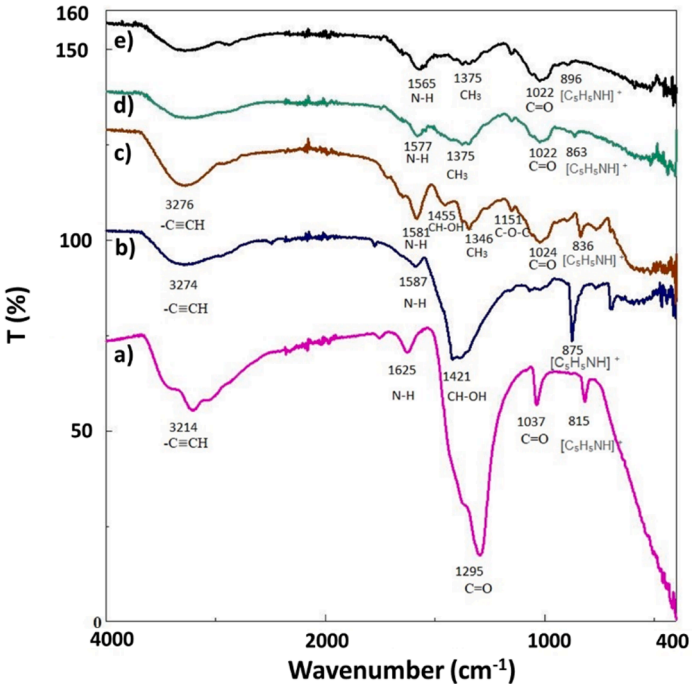

Fig. 1. FTIR spectrums of the BFO (a), 6% CHT (b), 6% CHT/0.025% BFO (c), 6% CHT/0.05% BFO (d), and 6% CHT/0.075% BFO (e).

(Mitutoyo MTI Corp., USA).

2.5.5. X-Ray diffraction (XRD)

XRD machine was used to obtain the crystal structure of BFO powders and 3D-printed scaffolds. In this test, Cu source ($\lambda = 1.54060$ A°) was used to obtain the X-rays. The scan range was adjusted to 10 to 90° and the scan rate was adjusted to 2°/min.

2.5.6. Cell viability analysis and SEM imaging of Cell-Seeded scaffolds

For the analysis of cytotoxicity of scaffolds on mouse embryonic fibroblasts (NIH 3 T3) MTT assay was performed on days 1, 4, and 7 of cell culture. Prior to cell seeding, the scaffolds were transferred to 96-well plates and sterilized with ethanol, and then washed with PBS and finally with culture media. Fibroblasts were seeded with a density of 10,000 cells/scaffold in a 96-well plate. After 24, 96, and 168 h of cell seeding, cell viability analysis was carried out according to the manufacturer's protocol. Briefly, the culture media of the samples were replaced with fresh media containing 5 mg/mL MTT (Vybrant MTT Cell Proliferation Assay Kit, Thermo Fischer Scientific), and then the samples were incubated for 4 h in a CO_2 incubator. To dissolve the formazan crystals formed as the reduction of MTT after 4 h-incubation, sodium dodecyl sulfate (SDS) was added into each well and incubated at 37 ∘C for 12 h. The optical density of each sample was measured at 570 and 630 nm by using a microplate reader (Biotek, Winooski, VT, USA). The experiment was performed three times (n = 3). Percent cell viability was calculated using the following formula (1).

$$\text{Cell Viability (\%)} = (\text{OD test/OD control}) \times 100 \quad (1)$$

The morphology of the cells on the scaffolds was examined by SEM. The cell-seeded scaffolds were washed with cacodylate buffer (0.1 M, pH 7.4) and then fixed with 4% glutaraldehyde. Dehydration was performed with serial dilutions of ethanol. Finally, scaffolds were air-dried and then coated with gold for 20 s prior to SEM analysis. The attachment and viability of fibroblast cells on the scaffolds were examined by acridine orange staining. After 1, 4, and 7 days of incubation, the growth medium of the cells was removed and the medium was cleaned with PBS. Then, the scaffolds were fixed with 4% paraformaldehyde for 30 min at room temperature and washed with PBS. After cleaning with PBS, 6 μg/ml acridine orange was added to each scaffold and incubated at room temperature for 10 min. Then, the acridine orange solution was discarded and the scaffolds were washed three times with PBS.

2.5.7. Drug release behavior of the AMX from the scaffolds

The AMX release from the scaffolds was examined in phosphate-buffered saline (PBS, pH:7.4) at 37 °C. The resultant AMX concentration was detected with a UV–Vis spectrophotometer (Shimadzu, Tokyo, Japan) at various time intervals. The calibration curve of the AMX was determined over a wavelength range of 190–500 nm and five different AMX concentrations (0.25, 0.5, 1, 1.5, and 2 μg/ml). In the drug release test, firstly 5 mg of AMX-loaded scaffolds were weighed and dissolved with 1 ml PBS (pH:7.4) in Eppendorf tubes. The absorbance values of the AMX were detected at different time intervals. Fresh PBS was used after each measurement. The AMX release was determined at 230 nm.

2.5.8. Electrically controlled AMX release from the scaffolds

In the 'electrically controlled drug delivery' step, an OTA-CFA-based changeable pulse generator is utilized to observe the electric effect on AMX release at 50 Hz frequency value. This circuit contains the square waveform generator, operational transconductional amplifier (OTA), and current-feedback amplifier (CFA). The details of the circuit are given in a previous article carried out by Gunduz et al [10]. After the system was set up, nearly 5 mg of all scaffolds were weighed and placed on the Eppendorf tubes with PBS (pH 7.4). The Ag/Pt electrode was used to transfer the electricity to the PBS (1 ml) in the eppendorf tube. The experiment was carried out at 50 Hz frequency and 10 V conditions. The electricity was applied to the scaffolds for different time intervals. After the application of an electric field, the PBS was taken from the Eppendorf tubes and absorbance values were detected at a wavelength of 230 nm.

2.5.9. Swelling and degradation properties of the scaffolds

In the swelling test, all experimental groups were placed in 1 ml phosphate buffer saline (PBS) with pH 7.4. The scaffolds were held in a thermal shaker (BIOSAN TS-100) at 37 °C with 300 rpm. The initial weights (W_0) and the wet weights (W_w) of the scaffolds were measured daily. The swelling rate (SR) was measured with equation (2).

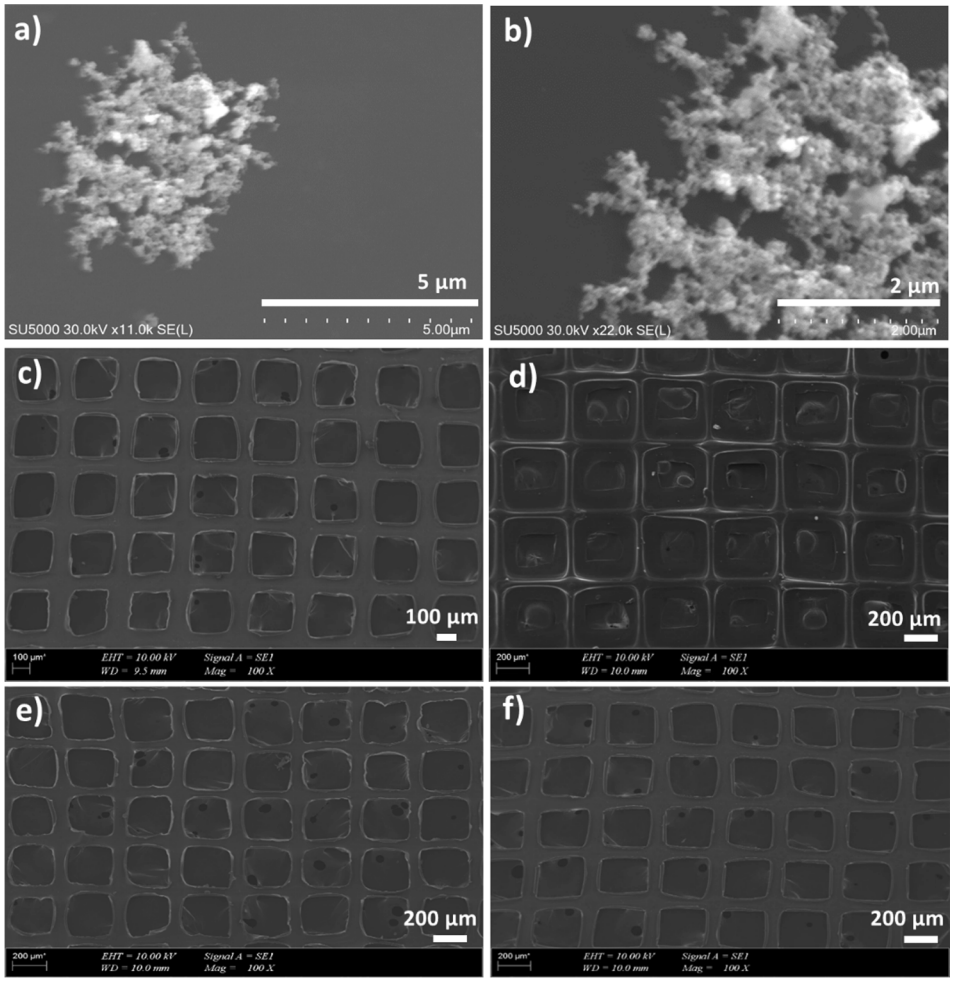

Fig. 2. The TEM images of the BFO particles (a, b), the SEM images of the 3D-printed scaffolds, 6% CHT (c), 6% CHT/0.025% BFO (d), 6% CHT/0.05% BFO (e), and 6% CHT/0.075% BFO (f).

$$SR = \frac{W_w - W_0}{W_0}.100 \quad (2)$$

In the degradation test, the same procedure was used with swelling test. However after the incubation, he scaffolds were removed from PBS medium and dried in an incubator at 37 °C for 24 h and the dried form weighed (W_t). The degradation rate (DR) was calculated by using equation (3).

$$DR = \frac{W_0 - W_t}{W_0}.100 \quad (3)$$

3. Results and discussions

To investigate the interaction of chemical and molecular structure in produced CHT scaffolds, FT-IR analysis was carried out on the four groups. These scaffolds that were containing different concentrations of BFO, present the following specific vibrations: the characteristic absorption bands at 1565 cm^{-1}, 1375 cm^{-1}852 cm^{-1}, which are associated with familiar vibrations for C≡CH, N–H and saccharide [14]. The distinctive peak is in the absorption band at 815 cm^{-1} in the spectrum for all experimental groups. The glycosidic bond is the strongest peak in the entire spectrum (Fig. 1 e). The characteristic bands of drug loaded BFO were observed with a C = O vibration peak at 1295 cm^{-1}. A band, corresponding to the vibration of N–N stretching was found at 1625 cm^{-1}, C = O stretching at 1037 cm^{-1} (Fig. 1 (b, c)). For pure CHT, related peaks were found at 3283 cm^{-1} representing the N–H stretching, C–H vibration at 2869 cm^{-1}, and primary amide C = O stretching at 1589 cm^{-1} (Fig. 1 d) [15]. For chitosan and bismuth ferrite combination groups, the absorption bands were observed at ~1577 cm^{-1}, 1375 cm^{-1}, 1022 cm^{-1}, and 863 cm^{-1}. These results indicate that molecular bonds of the pure CHT and AMX-loaded BFO are found in combinations.

Porosity is important for controlling the rate of drug release, while surface roughness affects the adhesion of cells and proteins. The viscosity of the 3D printing ink has a major effect on the final 3D printed structure. Low viscosity can cause the chitosan ink to flow too quickly and create a rough surface finish or drooping layers. On the other hand, a viscosity that is too high can cause clogging of the nozzle and disruption to the printing process. Chitosan with high molecular weight chitosan may result in greater strength and stiffness of the printed product. The concentration of the nanoparticles in the ink may also affect the resolution and accuracy of the printed product. Furthermore, the BFO nanoparticles can increase the porosity of the 3D printed part, which can be beneficial for applications such as drug delivery or tissue engineering.

Knowing that BFO is a ferroelectric material with a high piezoelectric response it can be used to generate an electric field in the composite. This electric field can help to promote cell attachment and spreading, as well as the supporting the adhesion of cells to the biopolymer. It could also alter the behavior of the cells, by inducing changes in the expression of certain genes and proteins [16]. In addition, the electric field may also affect the properties of the biopolymer, such as its mechanical strength, chemical stability, and biocompatibility. Thus, adding BFO to a biopolymer composite can significantly impact cell attachment and behavior of the final composite.

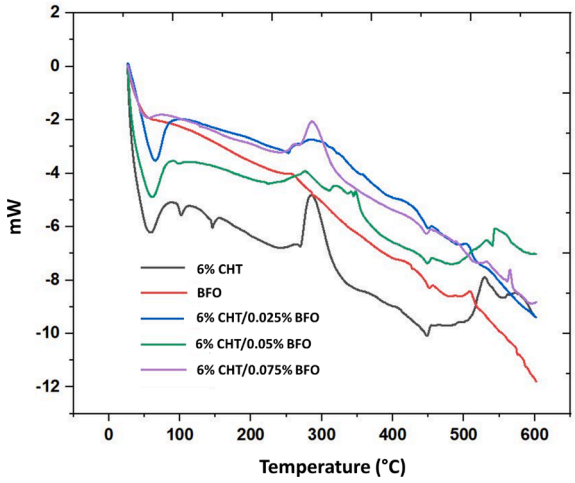

Fig. 3. DSC curves of the synthesized BFO and 3D-printed scaffolds.

Table 1
Tensile strength and strain values of the dry 3D printed scaffolds.

Scaffolds	Tensile strength (MPa)	Strain at break (%)
6% CHT	4.01 ± 1.04	5.34 ± 0.82
6% CHT/0.025% BFO	4.97 ± 0.34	12.09 ± 4.73
6% CHT/0.05% BFO	4.61 ± 1.38	7.59 ± 1.73
6% CHT/0.075% BFO	3.08 ± 0.77	10.09 ± 0.19

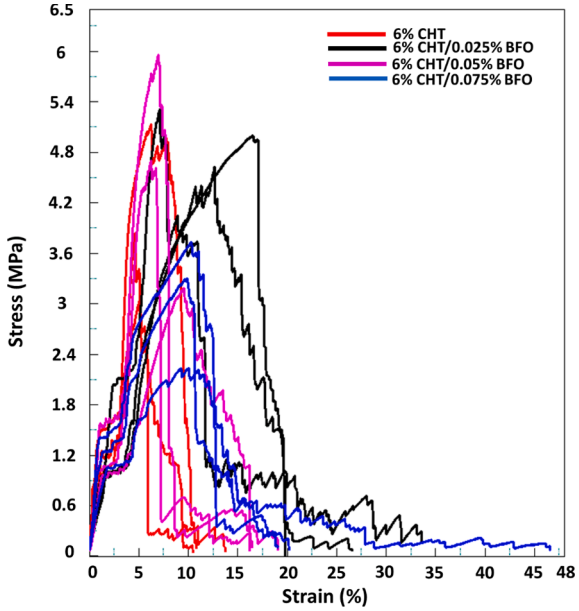

Fig. 4. The stress–strain curve of the 3D-printed scaffolds.

Fig. 2 (a, b) represents the TEM images of the BFO particles. In the TEM images, uniformly formed nanoparticles can be seen. The morphologies of the particles show that they are agglomerated with an almost spherical shape. This agglomeration can be attributed to the co-precipitation method, which produces particles of very small size [17].

Fig. 2 (c-f) highlights the morphology of the fabricated scaffolds at two different magnifications (100X and 200X), with all structures characterized by a well-defined geometry and structure, indicating the control and fidelity of the scaffold fabrication process.

The DSC curves of BFO (loaded with amoxicillin) and the 3D-printed

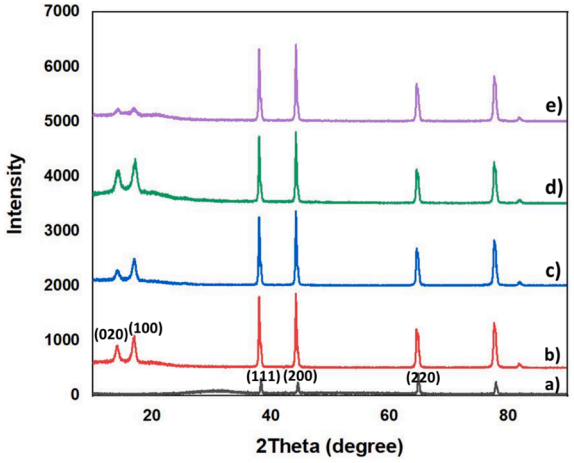

Fig. 5. XRD peaks of the synthesized BFO (a), 6% CHT (b), 6% CHT/0.025% BFO (c), 6% CHT/0.05% BFO (d), and 6% CHT/0.075% BFO (e) scaffolds.

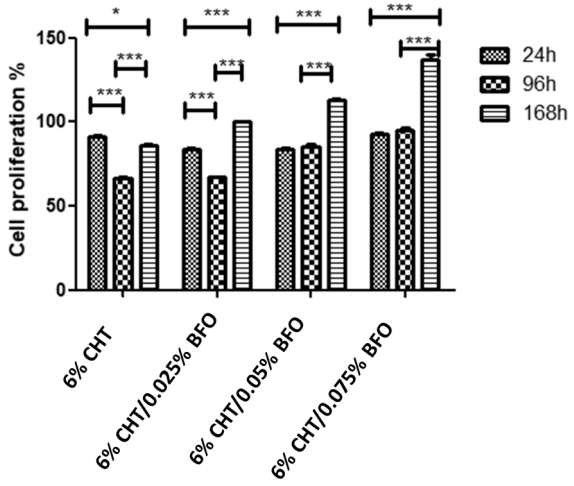

Fig. 6. MTT graph of the 3D-printed scaffolds after 24, 96, and 168 h of culture period with fibroblast cells.

scaffolds are presented in Fig. 3. It was observed that a minor endothermic peak as a result of dehydration of AMX occurs at ~ 100 °C. A minor broad endothermic peak, due to AMX fusion degradation at 190-~222.3C was also observed [18]. Fig. 3 shows that a steep exothermal peak occurs at ~ 230 °C, which is attributed to a mass loss of the BFO due to its decomposition to $Fe(OH)_3$ and $Bi(OH)_3$ metastable states [12]. These metastable states of $Bi(OH)_3$ and $Fe(OH)_3$ are subsequently transformed to stable Bi_2O_3 and Fe_2O_3 phases, respectively [12]. The stable phases (i.e. Bi_2O_3, Fe_2O_3 phases) further decompose at ~ 570 °C, as highlighted by the weak peak observed. The additional phase transition of BFO at curie temperature (830C) was not observed due to the temperature limit (600 °C) of the equipment employed in the present study [12]. The DSC of the 6% CHT scaffold also highlighted some characteristic endothermic peaks at ~ 50 °C, ~92 °C and ~ 150 °C which may be due to the evaporation of the residual solvent (i.e. acetic acid) employed during scaffold preparation. These peaks are also present in the DSC curves of 6% CHT/0.025% BFO, 6% CHT/0.05% BFO, and 6% CHT/0.075% BFO, albeit diminished, as the BFO concentration becomes progressively higher. An exothermic peak was observed at ~ 270° C, which is associated with the depolymerization, dehydration of the saccharide ring, and deacetylated and acetylated chitosan units decomposition [19]. Due to this degradation, the melting temperature was not observed. Indeed, it was reported that the amorphous region in the chitosan results in the dispersion of the energy points [19]. As

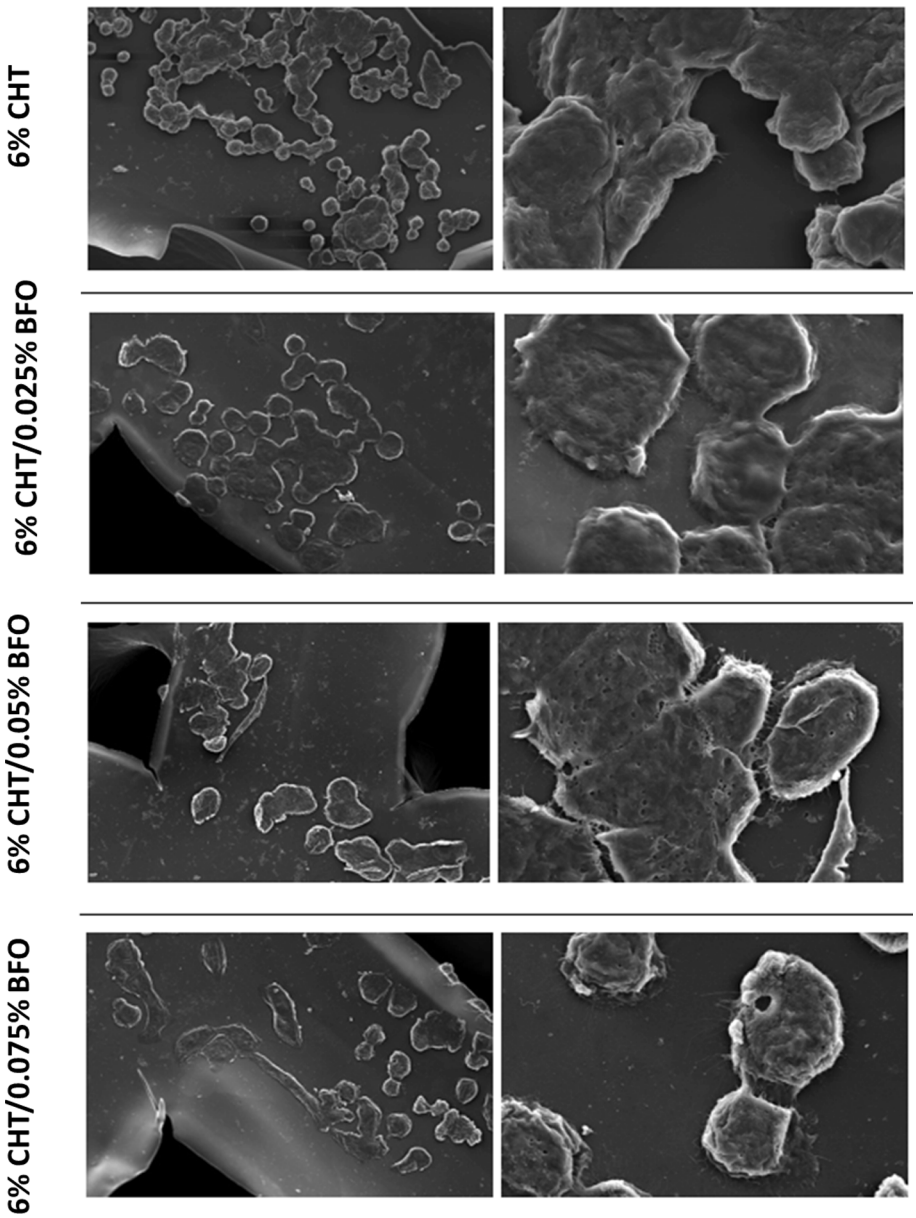

Fig. 7. SEM images of the 3D-printed scaffolds after 7 days of incubation.

expected, other chitosan-based scaffolds also presented similar decomposition peaks, which were observed to be less intense as the concentration of the BFO was progressively increased.

The tensile strength of a 3D-printed chitosan scaffold is an important factor for determining its biocompatibility and suitability for tissue engineering applications. Strain at break and tensile strength are two important parameters used to evaluate the mechanical properties of 3D-printed natural polymer scaffolds. The strain at break is a measure of the scaffold's ability to withstand an applied load before it fails. It measures the degree of deformation a scaffold can withstand before it permanently deforms or breaks. The tensile strength is a measure of the amount of force required to break the scaffold.

The tensile strength of 3D printed chitosan scaffold is largely determined by the type of printing process used, the concentration of chitosan in the 3D printing medium, and the type of solvent and crosslinker. Additionally, the use of a higher concentration of chitosan in the 3D printing medium can increase tensile strength. The tensile strength of 3D printed chitosan scaffold can also be improved through the addition of reinforcing agents such as carbon nanotubes and graphene [20–22]. These materials can be used to increase the tensile strength of the scaffold by increasing the intermolecular interactions between the chitosan molecules and reinforcing agents. In this study, by the addition of 0.025% of BFO to the scaffold formulation, the tensile strength and strain at break of the scaffolds increased. We observed about 1 MPa increase in tensile strength and about 7% in the strain at break, however, further increase of BFO (>0.025%) had a negative impact on the tested parameters (Table 1 and Fig. 4). Therefore a balanced concentration of BFO could improve the mechanical properties of the scaffold.

Fig. 5 shows the XRD patterns of scaffolds for the assessment of the crystalline phases present. To this regard, the XRD patterns of the scaffolds, based on BFO, 6% CHT, 6% CHT/0.025% BFO, 6% CHT/0.05% BFO, and 6% CHT/0.075% BFO and designated as Fig. 5 (a),(b), (c), (d) and (e) respectively were presented. Fig. 5 shows that the major diffraction peaks at 2θ angles of 39.41°, 45.68°, 65.9° and 76° were observed in the XRD of BFO (Fig. 5 a). These peaks are consistent with some of the major peaks of the XRD pattern of single-phase BFO with a distorted perovskite structure [23]. However, other peaks at 2θ angles of 22.34°, 27.6°, 31.68°, 32°, 51.24°, and 57.1° that characterize

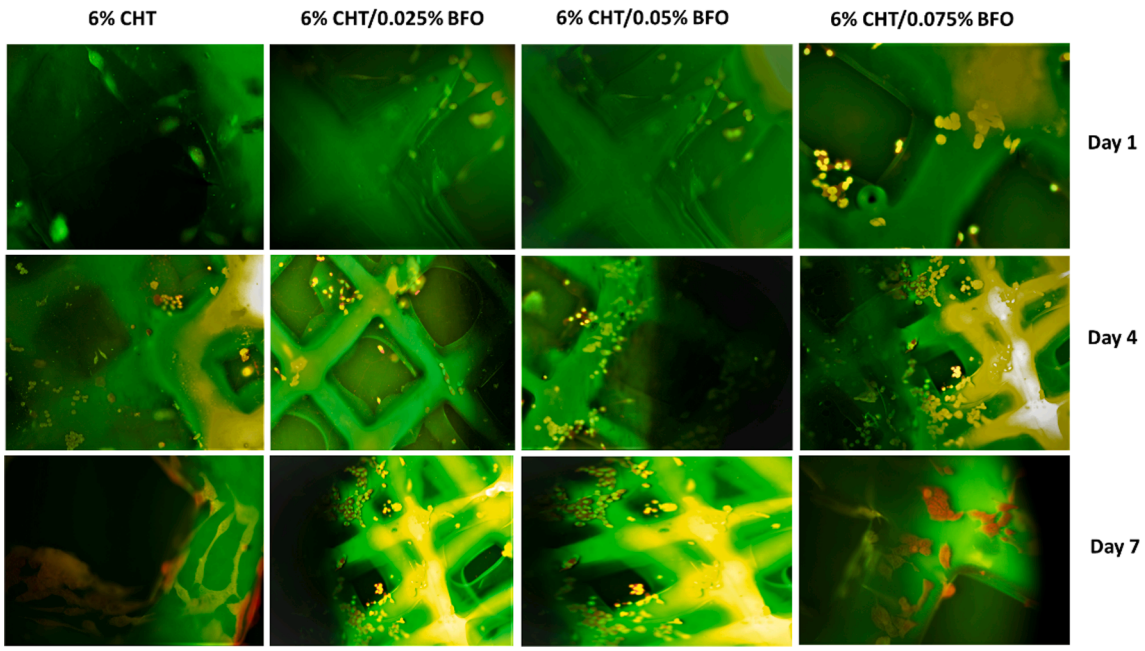

Fig. 8. Fluorescence images of the scaffolds after 1, 4, and 7 days of culture period.

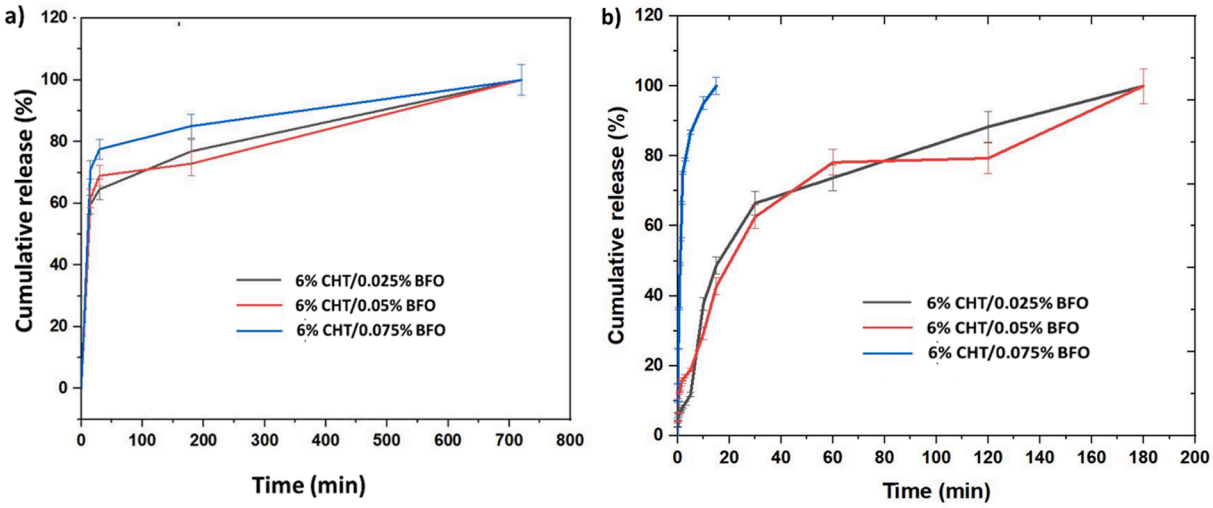

Fig. 9. Drug release behaviors of the AMX from the scaffolds, without electric field (a), under electric field (b).

crystalline BFO nanoparticles according to (JCPDS Card No. 86–1518) were absent [23]. This suggests the reduced crystallinity of the BFO prepared in the present study. This observation is expected since the 'as prepared' BFO sample (i.e. without further treatment) has been reported to present a mainly amorphous nature [24]. This outcome may be due to the low temperature imposed during the preparation approach and the absence of the calcification step. Notably, the low temperature imposed in the BFO preparation approach may explain the absence of impurity peaks. This is because, the application of low temperatures (i.e. $< 450\ ^{\circ}C$ [25]) may reduce the risk of secondary impurity peaks such as $Bi_{36}Fe_2O_{57}$ and $Bi_3Fe_4O_9$ typically detected at $2\theta = 29.39^{\circ}$, 25.69° and 34.12° [25]. Crucially, the absence of the characteristic peaks of amoxicillin reported to typically occur at 2θ angles of 18.1°, 19.5°, 23.1°, 26.4° and 28.3° [26] in the XRD pattern presented in Fig. 5 (a) may be due to its low concentration. Indeed, the literature suggests that if the concentration of BFO is higher than the concentration of amoxicillin, the XRD patterns due to BFO may be sufficient to dispel X-rays, leading to a weaker signal overall [27]. Amoxicillin drug presence will therefore be demonstrated using additional tests (i.e. drug release kinetics etc.) as discussed in subsequent sections. Fig. 5 also shows that the 6 % CHT sample presents peaks in 2θ at 10.5° and 19.8°, which are associated with the (020) and (100) crystallographic planes, respectively. These peaks are indicative of the typical chitosan structure [28]. Notably, in the XRDs for the scaffolds of Fig. 5 (b), (c), (d), and (e), the intensity of the peaks in 2θ at $10.5^{\circ}$and 19.8° is slightly diminished when compared to the XRD of pure chitosan reported in the literature [29]. The reduced intensity of the peaks may be due to the application of acetic acid in the preparation of the 6% CHT solution since the acetic acid has the potential of breaking down the crystal regions present in chitosan when it is dissolved [30].

Fig. 6 shows the quantitative analysis of cell viability in the presence of the different scaffolds based on 6% CHT, 6% CHT/0.025% BFO, 6% CHT/0.05% BFO, and 6% CHT/0.075% BFO, using the MTT assay. It was observed that, after 24 h of culturing the cell proliferation in all scaffolds was comparable. Notably for 6% CHT and 6% CHT/0.025% scaffolds, the cell proliferation at 96 h was less than the cell proliferation

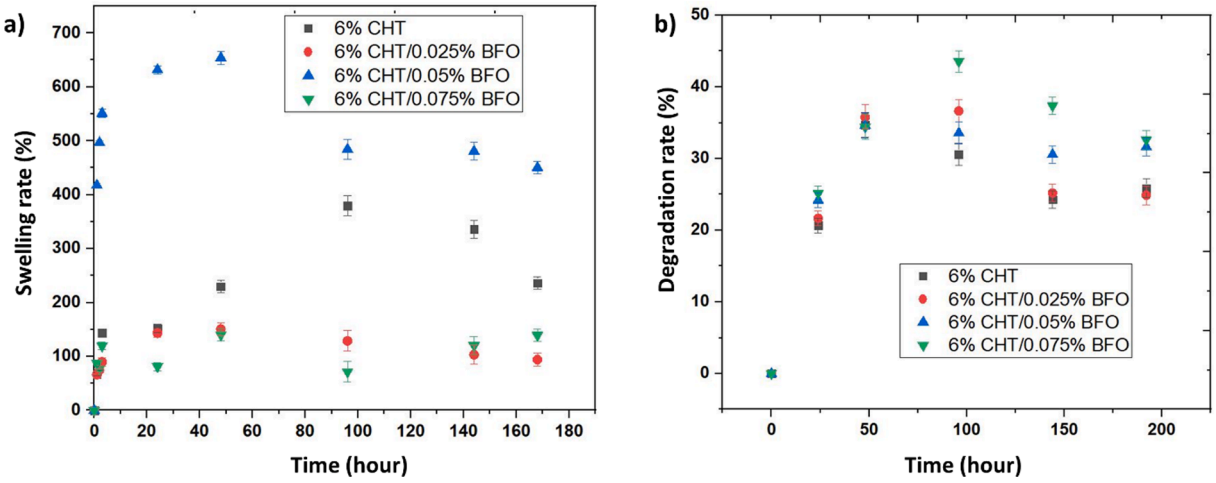

Fig. 10. Swelling and degradation profiles of the 3D-printed scaffolds.

at 24 h. This observation may be indicative of the requirement for the cell to attain the necessary stationary phase due to the increased surface area available for proliferation as the BFO content increases [31]. Fig. 6 also shows a positive correlation between the cell proliferation and the BFO content after 96 h and 168 h of cultivation. This enhanced cell proliferation is reinforced in the SEMs (Fig. 7) and is due to the increase in the overall porosity of the scaffolds by cause of higher concentrations of BFO nanoparticles. Indeed, the poor cell proliferation in the CHT scaffold could be because of the low porosity which can hinder cell anchorage and adhesion, even leading to cell death [32]. The enhanced cell proliferation of the scaffold with increasing BFO content is observed in Fig. 7 with the increase in the concentration of BFO nanoparticles contributing to the roughness of the scaffold surface. The increased surface roughness enables the cells to attach to the matrix with the cells subsequently dividing to form non-uniform cell clumps. Fig. 8 shows the fluorescence images of the scaffolds after 1, 4, and 7 days of incubation and results showed that the cell distribution was higher for all scaffolds than the cell distribution obtained on 1st day.

The results of our drug release studies indicate that the addition of BFO can significantly enhance the release rate of the drug from the chitosan composite (Fig. 9a). This is attributed to the presence of nanoparticles, which create a large surface area for drug adsorption and release. Additionally, the magnetic properties of BFO can be used to control the drug release rate and direction, allowing the drug to be released in a controlled manner. The incorporation of BFO into the chitosan composite increased the AMX drug release rate by reducing the particle size and increasing the porosity of the composite. The smaller particle size of BFO allows for greater drug diffusion through the composite, resulting in an increased release rate. Additionally, the enhanced porosity of the composite due to the incorporation of BFO expands the surface area for drug diffusion and thus increases the drug release rate. In addition, BFO can also modulate the release of AMX by its ferroelectric properties. The ferroelectric properties of BFO allow for the application of an electric field which can be used to control the release rate of AMX. The electric field affects the orientation of the dipoles in the BFO, thus changing the porosity of the composite and resulting in increased or decreased release of the drug (Fig. 9b). According to the results, it can be said that by adjusting the applied current's characteristics, the delivery can be customized to the needs of the patient. Electrically triggered drug release also has the potential to get around some of the drawbacks of traditional drug delivery methods, such as low drug efficacy and possible adverse effects [33].

The swelling and degradation profiles of the scaffolds were given in Fig. 10 (a, b). To protect the wound from infections, an ideal wound dressing must maintain a moist environment while absorbing wound fluids [34]. The swelling rates of the scaffolds were showed in Fig. 10a. The all 3D-printed scaffolds were exhibit a swelling profile up to the 4th day. The 6% CHT/0.025% BFO and 6% CHT/0.075% BFO scaffolds exhibited similar swelling rates and it was lower than the swelling rate value of 6% CHT scaffold. The reason for the high swelling rate of chitosan may be its porous structure [12]. The 3D-printed scaffolds were started to degrade on the 6th day. Saatcioglu et al. fabricated Chitosan/Osage orange extract scaffolds and reported that the highest swelling ratio was belonged to the only 6% CHT scaffold [12]. The 3D-printed scaffolds were exposed to PBS and weight loss over time was recorded. The degradation rates of 6% CHT, 6% CHT/0.025% BFO, 6% CHT/0.05% BFO, and 6% CHT/0.075% BFO scaffolds were showed in Fig. 10b. For the first 48 h, the scaffolds loss nearly 35% of their weights. According to the results, all the scaffolds were exhibited proportional degradation profile.

4. Conclusions

This study demonstrated the feasibility of using 3D printing technology to fabricate a chitosan-based wound dressing with the addition of bismuth ferrite (BFO) nanoparticles. BFO loaded chitosan based scaffolds were characterized physicochemically and results showed that BFO nanoparticles were successfully loaded into the chitosan scaffolds. SEM imaging showed that the BFO nanoparticles increased the porosity of the 3D printed scaffolds that improves drug release profile and good for cell attachment with high biocompability. The drug release rate of amoxicillin from the composite was significantly enhanced with the addition of BFO, which can be attributed to the small particle size and increased porosity of the composite. Additionally, the incorporation of BFO increased the mechanical strength and strain at break of the the 6% CHT scaffold, which is important for tissue engineering applications. The results of fibroblast culturing showed that the cells successfully adhered onto scaffolds and maximum cell viability was observed for 6% CHT/0.075% BFO scaffolds. Finally, the ferroelectric properties of BFO can be used to modulate the release of AMX by applying an electric field (10 V, 50 Hz), thus providing a controlled release system, suggesting that AMX release could be controlled with the application of electricity. This study demonstrates the potential of using 3D-printed chitosan scaffolds with BFO nanoparticles for controlled drug delivery in wound dressings. The printed chitosan based scaffolds that improved as electrically conductive, can be used in triggered drug relase applications. In this manner, controlled drug release enhanses the wound healing to a visible extent.

Data availability.

The raw data will be made available upon request.

Declaration of Competing Interest

The authors declare that they have no known competing financial interests or personal relationships that could have appeared to influence the work reported in this paper.

Data availability

Data will be made available on request.

References

[1] E.I. Shishatskaya, et al., Experimental wound dressings of degradable PHA for skin defect repair, J. Mater. Sci. - Mater. Med. (2016) 27 (11).
[2] T. Bedir, S. Ulag, C.B. Ustundag, O. Gunduz, 3D bioprinting applications in neural tissue engineering for spinal cord injury repair, Mater. Sci. Eng. C, 110 (2020), 110741.
[3] S. Agila, J. Poornima, Magnetically controlled nano-composite based 3D printed cell scaffolds as targeted drug delivery systems for cancer therapy, in: IEEE 15th International Conference on Nanotechnology (IEEE-NANO), 2015.
[4] M. Ayran, H. Karabulut, K.I. Deniz, G.C. Akcanli, S. Ulag, A.-M. Croitoru, B.-M. Tihăuan, A. Sahin, D. Ficai, O. Gunduz, A. Ficai, Electrically triggered quercetin release from polycaprolactone/bismuth ferrite microfibrous scaffold for skeletal muscle tissue, Pharmaceutics 15 (3) (2023) 920.
[5] S. Li, J. Zhang, M.G. Kibria, Z. Mi, M. Chaker, D. Ma, R. Nechache, F. Rosei, Remarkably enhanced photocatalytic activity of laser ablated Au nanoparticle decorated BiFeO3 nanowires under visible-light, Chem. Commun. 49 (52) (2013) 5856e5858.
[6] F. Ajalloueian, et al., Amoxicillin-loaded multilayer pullulan-based nanofibers maintain long-term antibacterial properties with tunable release profile for topical skin delivery applications, Int. J. Biol. Macromol. 215 (2022) 413–423.
[7] K.C. Gupta, F.H. Jabrail, Glutaraldehyde cross-linked chitosan microspheres for controlled release of centchroman, Carbohydr Res. 342 (15) (2007) 2244–2252.
[8] J. Long, et al., A 3D printed chitosan-pectin hydrogel wound dressing for lidocaine hydrochloride delivery, Mater. Sci. Eng. C 104 (2019), 109873.
[9] R.C. Goy, et al., A review of the antimicrobial activity of chitosan, Polymers (Basel) 19 (3) (2009) 241–247.
[10] A.M. Croitoru, et al., Electrically Triggered Drug Delivery from Novel Electrospun Poly(Lactic Acid)/Graphene Oxide/Quercetin Fibrous Scaffolds for Wound Dressing Applications, Pharmaceutics 13 (2021) 957.
[11] S.E. Neumann, C.F. Chamberlayne, R.N. Zare, Electrically controlled drug release using pH-sensitive polymer films, Nanoscale 10 (2018) 10087–10093.
[12] S. Ulag, et al., Fabrication of three-dimensional PCL/BiFeO3 scaffolds for biomedical applications, Mater. Sci. Eng. B 261 (2020), 114660.
[13] E. Saatcioglu, M. Koyun, S. Ulag, A. Sahin, B.K. Yilmaz, B. Aksu, et al., 3D printing of Osage orange extract/Chitosan scaffolds for soft tissue engineering, Food Hydrocoll Heal. 1 (1) (2021 Jan), 100039.
[14] T. Bedir, et al., Effect of electric stimulus on human adipose-derived mesenchymal stem cells cultured in 3D-printed scaffolds, Polym. Adv. Technol. 32 (3) (2020) 1114–1125.
[15] E. Saatcioglu, et al., Design and fabrication of electrospun polycaprolactone/chitosan scaffolds for ligament regeneration, Eur. Polym. J. 148 (2021), 110357.
[16] K. Krawczyk, et al., Electrogenetic cellular insulin release for real-time glycemic control in type 1 diabetic mice, Science 368 (2020) 993–1001.
[17] E. Juwita, F.A. Sulistiani, M.Y. Darmawan, N.I. Istiqomah, andEdi Suharyadi, Microstructural, optical, and magnetic properties and specificabsorption rate of bismuth ferrite/SiO2 nanoparticles, Mater. Res. Express 9 (2022), 076101.
[18] H. Maswadeh, Incompatibility of Paracetamol with Pediatric Suspensions Containing Amoxicillin, Azithromycin and Cefuroxime Axetil, Pharmacology & Pharmacy 8 (11) (2017) 355.
[19] S. Acosta-Ferreira, et al., Production and physicochemical characterization of chitosan for harvesting wild microalgae consortia, Biotechnol. Rep, 28 (2020) e00554.
[20] X. Pei, et al., Porous network carbon nanotubes/chitosan 3D printed composites based on ball milling for electromagnetic shielding, Compos. A Appl. Sci. Manuf. 145 (2021), 106363.
[21] L. Suo, et al., The improvement of periodontal tissue regeneration using a 3D-printed carbon nanotube/chitosan/sodium alginate composite scaffold, J. Biomed. Mater. Res. B Appl. Biomater. 111 (1) (2023) 73–84.
[22] L. Suo, et al., Improvement of osteogenic properties using a 3D-printed graphene oxide/hyaluronic acid/chitosan composite scaffold, J. Bioact. Compat. Polym. 37 (4) (2022) 267–283.
[23] S.L. Agrawal, et al., Studies on multiferroic oxide-doped PVA-based nanocomposite gel polymer electrolyte system for electrochemical device application, Ionics 25 (2) (2019) 617–626.
[24] P. Reddy Vanga, R.V. Mangalaraja, M. Ashok, Structural, magnetic and photocatalytic properties of La and alkaline co-doped BiFeO3 nanoparticles, Mater. Sci. Semicond. Process. 40 (2015) 796–802.
[25] A. Manzoor, et al., Synthesis and characterization of Bismuth ferrite (BiFeO3) nanoparticles by solution evaporation method, J. Magn. Magn. Mater. 393 (2015) 269–272.
[26] Rehmat, M., *Crystallization of Amoxicillin in Presence of Denatured Impurities and their Effect on Crystallization.* 2022.
[27] Q. Li, et al., Ag modified bismuth ferrite nanospheres as a chlorine gas sensor, RSC Adv 8 (58) (2018) 33156–33163.
[28] S. Kumar, J. Koh, Physiochemical, the optical and biological activity of chitosan-chromone derivative for biomedical applications, Int J Mol Sci 13 (5) (2012) 6102–6116.
[29] T.A. Phung Hai, R. Sugimoto, Fluorescence control of chitin and chitosan fabricated via surface functionalization using direct oxidative polymerization, RSC Adv. 8 (13) (2018) 7005–7013.
[30] B. Ma, et al., New binary ionic liquid system for the preparation of chitosan/cellulose composite fibers, Carbohydr. Polym. 88 (1) (2012) 347–351.
[31] S. Bhat, A. Kumar, Cell proliferation on three-dimensional chitosan–agarose–gelatin cryogel scaffolds for tissue engineering applications, J. Biosci. Bioeng. 114 (6) (2012) 663–670.
[32] R. Mahdavi, et al., Bone tissue engineering gelatin–hydroxyapatite/graphene oxide scaffolds with the ability to release vitamin D: fabrication, characterization, and in vitro study, J. Mater. Sci. - Mater. Med. 31 (11) (2020) 97.
[33] S. Adepu, S. Ramakrishna, Controlled drug delivery systems: current status and future directions, Molecules 26 (2021) 5905.
[34] E. Altan, N. Turker, O.A. Hindy, Z. Dirican, O.B. Ozakpinar, A.U. Demir, et al., Investigation of 3D-printed chitosan-xanthan gum patches, Int. J. Biol. Macromol. 31 (213) (2022) 259–267.